Article

Efficient CH$_4$/CO$_2$ Gas Mixture Separation through Nanoporous Graphene Membrane Designs

Naiyer Razmara [1,*], Alexsandro Kirch [2], Julio Romano Meneghini [1] and Caetano Rodrigues Miranda [2]

[1] Department of Mechanical Engineering, Escola Politécnica, University of São Paulo, São Paulo 05315-970, SP, Brazil; jmenegh@usp.br
[2] Instituto de Física, Universidade de Sao Paulo, CP 66318, São Paulo 05315-970, SP, Brazil; alexsandro.kirch@usp.br (A.K.); c.miranda@usp.br (C.R.M.)
[*] Correspondence: n.razmara@usp.br

Abstract: Nanoporous graphene membranes have drawn special attention in the gas-separation processes due to their unique structure and properties. The complexity of the physical understanding of such membrane designs restricts their widespread use for gas-separation applications. In the present study, we strive to propose promising designs to face this technical challenge. In this regard, we investigated the permeation and separation of the mixture of adsorptive gases CO$_2$ and CH$_4$ through a two-stage bilayer sub-nanometer porous graphene membrane design using molecular dynamics simulation. A CH$_4$/CO$_2$ gashouse mixture with 80 mol% CH$_4$ composition was generated using the benchmarked force-fields and was forced to cross through the porous graphene membrane design by a constant piston velocity. Three chambers are considered to be feeding, transferring, and capturing to examine the permeation and separation of molecules under the effect of the two-stage membrane. The main objective is to investigate the multistage membrane and bilayer effect simultaneously. The permeation and separation of the CO$_2$ and CH$_4$ molecules while crossing through the membrane are significantly influenced by the pore offset distance (W) and the interlayer spacing (H) of the bilayer nanoporous graphene membrane. Linear configurations (W = 0 Å) and those with the offset distance of 10 Å and 20 Å were examined by varying the interlayer spacing between 8 Å, 12 Å, and 16 Å. The inline configuration with an interlayer spacing of 12 Å is the most effective design among the examined configurations in terms of optimum separation performance and high CO$_2$ and CH$_4$ permeability. Furthermore, increasing the interlayer distance to 16 Å results in bulk-like behavior rather than membrane-like behavior, indicating the optimum parameters for high selectivity and permeation. Our findings present an appropriate design for the effective separation of CH$_4$/CO$_2$ gas mixtures by testing novel nanoporous graphene configurations.

Keywords: separation; binary mixture; molecular dynamics; nanoporous graphene

1. Introduction

Due to growing greenhouse gases concentrations, especially carbon dioxide (CO$_2$) and methane (CH$_4$), global warming has recently become a major global issue. Since CO$_2$ is the most critical greenhouse gas released today, there have been many attempts to reduce CO$_2$-induced emissions. Using clean and environmentally sustainable manufacturing practices is a promising way to reduce the concentration of CO$_2$ in the atmosphere. One of these approaches is the implementation of Carbon Capture and Storage (CCS) systems. Given that CH$_4$ frequently coexists with CO$_2$ in gas mixtures such as natural gas, landfill gas, and biogas, CO$_2$ separation may be a critical process for improving these gas mixtures' energy content [1]. In the last decade, using nanotechnology in selective separation and eliminating pollutants has received considerable interest [2]. Highly innovative nanomaterials such as developed porous materials, porous organic polymers, and Metal-Organic Frameworks (MOF) have recently shown incredible potential in energy storage systems

owing to their unique surface area and tunable structures [3]. Among the latest materials of this kind, carbon-based materials have been extensively used for carbon capture because of their large availability, low cost, strong thermal and electrical conductivity, excellent thermal and chemical stability, and low sensitivity to humidity [4]. However, these materials also have drawbacks in the particular temperature and pressure ranges. Nanoporous carbon materials, carbon nanotubes (CNTs), and graphene-based materials are the predominant carbon-based materials. In particular, graphene has developed a promising nano-level platform with tremendous potential for application in various areas. Graphene membranes are a type of two-dimensional carbon membrane that has received a great deal of interest due to their excellent potential and monoatomic thickness. Using a graphene layer leads to enhancing permeability due to the inverse relationship between membrane permeability and membrane thickness [5]. Since pristine graphene is impermeable to helium and hydrogen [6], it is necessary to drill the pores to use graphene as a membrane. Such a pore-created graphene configuration is known as porous graphene that is a viable candidate for gas-separation membranes exhibiting ultra-high permeability. The main challenge in the development of these structures is the methods of creating pores in sub-nanometer dimensions and controlling their size. Despite the novelty of this issue, there are also advances in numerical and experimental research. These structures can be used to desalinate water [7,8], and separate gases [9].

The use of nanoporous graphene (NPG) in the separation of gases was first proposed by Sint, Wang, and Kral [10]. They used molecular dynamics (MD) to investigate the ion selectivity in graphene pores terminated by atoms that are either negatively charged or positively charged. It was shown that these membranes are highly selective for ions with lower radii. This study demonstrated two separation mechanisms for ionic separation, including size exclusion and electrostatic repulsion. In the field of ion separation, many continued to investigate the permeation rather than selectivity since the selectivity of these structures is proved computationally [10]. The second study using NPG for gas separation is conducted by Jiang, Cooper, and Dai [11], focusing on H_2/CH_4 gas's selectivity using Density Functional Theory (DFT). It demonstrated super efficiency in selectivity and permeability. It is one of the first examples showing a high-efficiency NPG membrane for gas separation. The graphene membrane has been widely investigated for both ion and gas separation thanks to the promising results of the numerical simulations mentioned above.

During the early stage of its development, substantial progress was made in using the NPG membrane for gas separation. Liu et al. [12], for example, performed MD simulation to demonstrate the porous graphene selectivity for $H_2/CO_2/N_2/Ar/CH_4$ due to size exclusion, especially for CO_2/N_2 separation. A comprehensive study was conducted by Tronci et al. [13] to evaluate the influence of pore size, shape, and functionalization on the gas-separation efficiency of NPG membrane. They discovered that pore shape plays an essential part in the gas-separation membrane based on gas molecules' asymmetric geometry. Raghavan and Gupta have further explored pore shapes' influence on gas-separation efficiency via MD, focusing exclusively on H_2/CH_4 separation [14]. They observed that gas permeance is heavily reliant on pore eccentricity by maintaining the pore area fixed. To obtain high H_2 permeance with high selectivity, an elliptical pore was found, filtering out most CH_4 molecules. Tronci et al. [13] have found that functionalization plays a pivotal role along with the shape. Higher affinity with edge functionalization of the gas molecules is associated with greater permeability. MD studies, therefore, show both the greater performance of NPG membranes for gas separation and the significance of pore design parameters, including size, shape, and functionalization. By comparing porous graphene and permselective membranes' performance, porous graphene is a viable structure for gas separation because it can potentially exceed other materials due to a high pore density [15]. Since the permeation of gas molecules through porous graphene becomes a rare event of a highly stochastic nature [16], simulating more suitable pore size and distribution on the graphene membrane designs is computationally cost-effective [17]. As a result, long simulation times and multiple trials are required to fully capture the

permeation and separation behavior, which results in low efficiency and accuracy in permeance estimations.

The separation of the binary mixture of CH_4/CO_2 is of significant importance because it is a critical stage in the natural gas industry [2] and has become one of the most well-researched membrane separation gas pairs [18]. Understanding the separation of methane and carbon dioxide at the nanoscale is of great importance for developing future applications in gas-separation processes. In particular, phenomena involving their mixture and confinement are of special interest in natural gas processing. We may contribute to the separation process optimization in carbon-based membranes within a broader phenomenological perspective provided by the multiscale molecular modeling framework from nano to the macroscopic scale.

In one of the first important studies in this field, Sun et al. [19] showed that high permeability and selectivity could be achieved to separate CH_4/CO_2, CH_4/H_2S, and CH_4/N_2 mixtures by NPG membranes with appropriate pore size and geometry. For the three gas mixtures, the separation efficiency of the NPG membranes far outperformed the upper bond of the traditional polymer membranes. In another important study by Sun and Bai [20], a negatively charged NPG membrane was suggested to improve CO_2/CH_4 gas mixture separation performance. The explanation behind this enhanced separation performance could be the relatively enhanced adsorption of CO_2 molecules and diminished adsorption of CH_4 molecules on the graphene surface at high partial charges. More recently, a comprehensive MD simulation was performed by Yuan et al. [15] to investigate the permeation of CO_2/CH_4 gas mixtures through porous graphene. A trade-off between CO_2 permeability and CO_2/CH_4 selectivity, represented by an upper bound for sub-nanometer hydrogen-terminated graphene pores in a Robeson plot, was revealed in the simulated results. Furthermore, Khakpay et al. [21] conducted MDS in single- and double-layered NPG and graphene oxide (GO) separation platforms to study the concentration-dependent adsorption and gas transport properties in a CH_4/CO_2 gas mixture. They showed that for both NPG and GO systems, the through-the-pore diffusion coefficients of both CO_2 and CH_4 increased with an increase in CH_4 concentration. The CO_2 permeability was shown to be lower than that of CH_4, indicating that both platforms are more suitable for CH_4/CO_2 rather than CO_2/CH_4 separation.

The development of NPG membranes relied heavily on computer simulations. Due to the complexity of physically fabricating and testing these membranes, theoretical research has made significant progress in this area. This could help with innovative design concepts, process optimization, or a deeper understanding of the separation or permeation mechanism. A feedback loop between the computational models and the experimental findings can be established as more experiment results are gathered. This contributes to the development of more practical computational models [22] for design optimization and scientific research. The scientists have put in a lot of effort to bring the NPG membrane principle to experimental tests. However, there has been limited progress owing to the complexity of creating precise nanopores [23,24].

The vast potential of NPG membranes for separation operations has been demonstrated by numerous simulation results. The feasibility of NPG membranes for separation with high permeability was also verified in subsequent experiments [25]. However, there is still a lot of work to be done to bring the idea to practical industrial processes [26]. Different theoretical and numerical simulations have shown that graphene-based membranes have a lot of potential to be used for gas separation [27]. The most critical parameter in controlling gas separation is the size of pores in graphene sheets.

Jiang et al. [11] were the first to introduce NPG as a gas-separation membrane that is atomically thin, highly functional, and selective. Others predicted that NPG could be used to purify methane as well as separate CO_2/N_2 or H_2/N_2 [28]. However, due to the complexity in accurately manipulating nanopores' size and distribution, few experimental findings exist in the literature. Koenig et al. [29] recently used UV-induced oxidative etching to build in-plane pores in micrometer-sized graphene membranes, which they

used as molecular sieves. The transport of various gases (H_2, CO_2, Ar, N_2, CH_4, and SF_6) through the pores was measured using a pressurized blister and mechanical resonance. The NPG showed molecular selectively and the measured leak rates decreased as molecular sizes increased.

Although the studies listed above provide a mechanistic understanding of gas permeation through graphene nanopores, studying hybrid and multistage configurations' efficiency remains a significant challenge. Only a few model NPG designs have been investigated in the scientific literature, which does not adequately characterize the real experimental graphene membranes. Because of the novelty of this research topic, there are few scientific studies on the separation of this binary mixture using porous graphene. However, after conducting a thorough analysis of the literature, some examples of current and useful work in this field were identified. Considering the foregoing, we aim to propose a novel membrane design based on two-stage bilayer porous graphene membranes. This design not only improves gas permeation efficiency but also improves selective separation performance. Furthermore, it has been demonstrated that by forming pores of various offset spacings, it is possible to track gas permeation through this porous graphene design. Hence, we explored the role of the most relevant design specifications, such as pore offset distance and interlayer spacing in terms of CH_4/CO_2 permeation and selectivity. The result obtained by MD simulation may provide some insight into the molecular behavior which could be useful in developing more efficient gas separation and storage processes. More research into nanoporous graphene-based membranes with other atoms or groups can be carried out by generalizing the conceptual framework developed in the literature and this paper.

2. Computational Method and Models

MD simulations were performed to examine the effect of applying two stages of bilayer graphene membranes on CH_4/CO_2 separation and permeation. The layout of the system that was built is divided into five parts. The first part, chamber (I), is the reservoir for the CH_4/CO_2 gas mixture, consisting of a graphene sheet that serves as a piston and makes the gas mixture go through the first graphene membrane. To avoid the impact of high velocity on the system's dynamic, a lower piston velocity was used and kept constant at 1m/s throughout the simulation process. The second and fourth divisions are the membranes composed of two porous graphene sheets with a pore radius of 4 Å with a designated interlayer spacing. Chamber (II) is the third part and serves as a transferring environment after the first stage of the gas-separation process. Chamber (III) is the fifth part of the system that acts as a capturing reservoir for the second stage of the gas-separation process. Three chambers, along with the two NPG membranes, are illustrated in Figure 1.
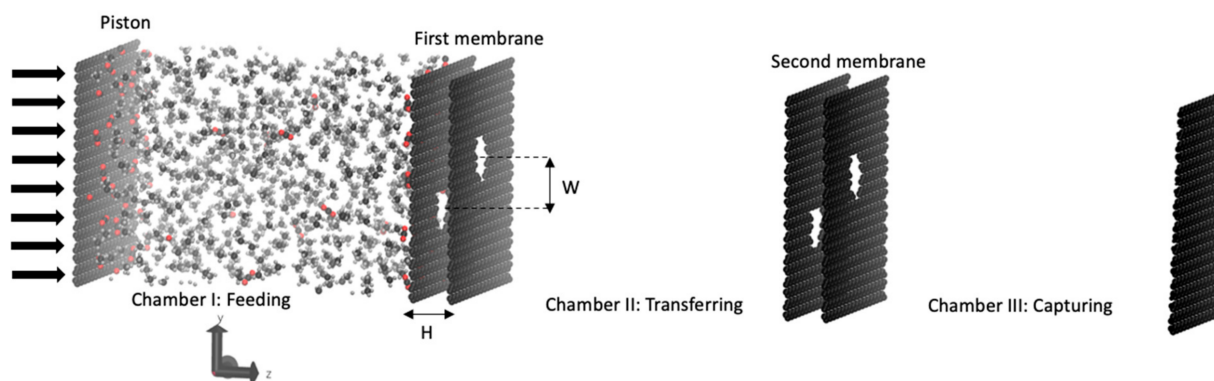
Figure 1. Initial configuration of the two-stage bilayer NPG membrane for CH_4/CO_2 separation.

Initially, a binary mixture of 20% CO_2 and 80% CH_4 with 27 CO_2 molecules and 297 CH_4 molecules was loaded into the left chamber, while both chambers on the right side were vacuum for all simulations. Inside the feeding chamber, the molecules of each gas

were randomly placed. The positions of the carbon atoms in the graphene sheets during the modeling process were set fixed to prevent the displacement of the graphene layers due to the pressure imposed by the gas molecules. In all three dimensions, periodic boundary conditions (PBC) were applied. Figure 1 displays the dimensions of various parts of the simulated system.

Benchmarked force-fields are adopted for modeling the interactions between different molecules. The most commonly used potential for CH_4 is the all-atom (AA) five-center semi-empirical Lennard–Jones (LJ) potentials, which provide the most precise definition of the fluid compared with other site–site potentials and suggested by Jorgensen et al. [30]. Hence, the all-atom optimized liquid simulation potential (OPLS-AA) is employed for CH_4 to capture important multi-body terms in interatomic interactions, namely bond stretching, bond angle bending, van der Waals, electrostatic interactions, and partial charges. On the other hand, the most frequently reported potential model for CO_2 is site–site interaction models, and a variety of potential models can be regarded as Elementary Physical Models (EPM) models for CO_2 [31]. Potoff and Siepmann [31] suggested the first variation of the EPM model, known as the abbreviation TraPPE. The TraPPE forcefield is used in this study for modeling CO_2 molecules. The graphene membranes are modeled with the Lennard–Jones potential. The parameters of the force field for gas molecules and graphene are tabulated in Table 1. The Lorentz-Berthelot mixing rule is employed for modeling the interactions among all cross-terms.

Table 1. Forcefield parameters for CO_2, CH_4, and graphene (q is the partial atomic charge; ε_{ab} is the maximum LJ energy of attraction between a pair of atoms; σ_{ab} is the collision diameter; r_0 is the equilibrium distance; θ_0 is the equilibrium angle; k_r is a harmonic force parameter for bond lengths; and k_θ a harmonic spring parameter for bond angles).

	Mass	q (e)	ε_{ab} (Kcal/mol)	σ_{ab} (Å)	r_0 (Å)	θ_0 (deg)	k_r (kJmol^{-1} Å^{-2})	k_θ (kJ mol^{-1} rad^{-2})
Graphene	12.001	0	0.070	3.984	-	-	-	-
CH_4-C	12.011	−0.24	0.066	3.500	1.09	107.8	2845.12	276.14
CH_4-H	1.008	+0.06	0.030	2.500				
CO_2-C	12.011	+0.70	0.053	2.800	1.16	180.0	8610.70	468.61
CO_2-O	15.999	−0.35	0.156	3.050				

To incorporate long-range electrostatic interactions, the Particle Mesh Ewald (PME) method was used. The equations of motion were integrated via a velocity Verlet method with a fixed time step of 0.1 fs. The energy minimization was carried out to determine the thermally stable structure and establish a configuration with all molecules' minimum potential energy. Each simulated system was pre-equilibrated for 20 ps to maintain the total energy and the temperature of systems stable. The Nose-Hoover thermostat and barostat were used to keep the temperature and pressure at 300 K and 1 atm, respectively. MD simulations were performed for 4ns to post-process the data in the production stage. In this study, the large-scale atomic/molecular massively parallel simulator (LAMMPS) package [32] was used to conduct simulations, and the atomic structures were visualized using the visual molecular dynamics (VMD) package.

3. Results and Discussion

The range of variation of parameters for pore size, the interlayer spacing, and pore offset distance has been selected according to the experimental findings in the literature review. As mentioned before, the size of pores in graphene sheets is the most important factor in the gas-separation performance of these membranes. Table 2 shows the experimental studies performed to create pores in the structure of graphene. Therefore, according to studies, choosing a pore radius of 4 Å is proven to be experimentally feasible.

**Table 2.** Summary of experimental studies on nanopore generation in graphene from the literature review.

Author (Year)	Surwade et al. [33]	Celebi et al. [34]	O'Hern et al. [35]	Koenig et al. [29]	Fan et al. [36]	Fox et al. [37]	Bieri et al. [38]	Fischbein et al. [39]
Pore size (nm)	~1	5–100	0.40 ± 0.24	0.4–10	~2.4	5.9 ± 0.4	~0.4	~3.5

Most studies on the use of graphene structures have focused on water desalination. Such research can, however, be applied to the separation mechanism of these membranes for gas separation. Based on experimental findings it was shown that the interlayer distance for GO varies with the amount of absorbed water, with values ranging from 0.63 nm and 0.61 nm for a dry sample to 1.2 nm for hydrated GO [40]. Hence, the interlayer spacing values used in our research, H = 8 Å, 12 Å, 16 Å, are experimentally feasible.

Furthermore, a combined experimental and molecular dynamics simulation study [41] was done to investigate the dependence of salt rejection efficiency and water permeability of layered GO membranes on the lateral dimension of constituting sheets. Pore offset distances of 0 Å, 4 Å, 8 Å, 16 Å, and 25 Å were investigated with different sizes of GO sheets. The pore offset distance or the size of the constituting GO sheets were found to be useful in fine-tuning the GO membrane's water permeation and salt rejection. Therefore, the examined values for the pore offset distance in our study, W = 0 Å, 10 Å, and 20 Å, are experimentally feasible.

An example of the visual observation of the permeation of CO_2 and CH_4 molecules through the given two-stage bilayer NPG membrane, instantaneous snapshots of the inline configuration (W = 0 Å) with the interlayer spacing of 8 Å are shown at five different simulation times in Figure 2.

(a)

(b)

(c)
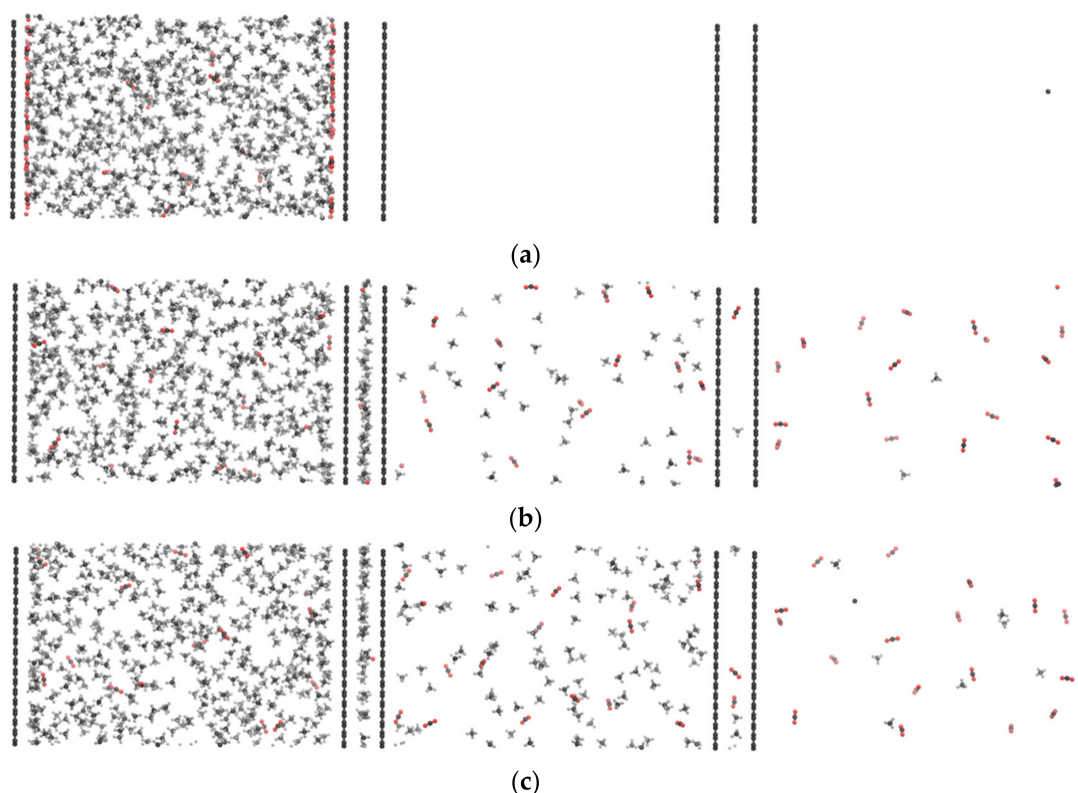
Figure 2. *Cont.*
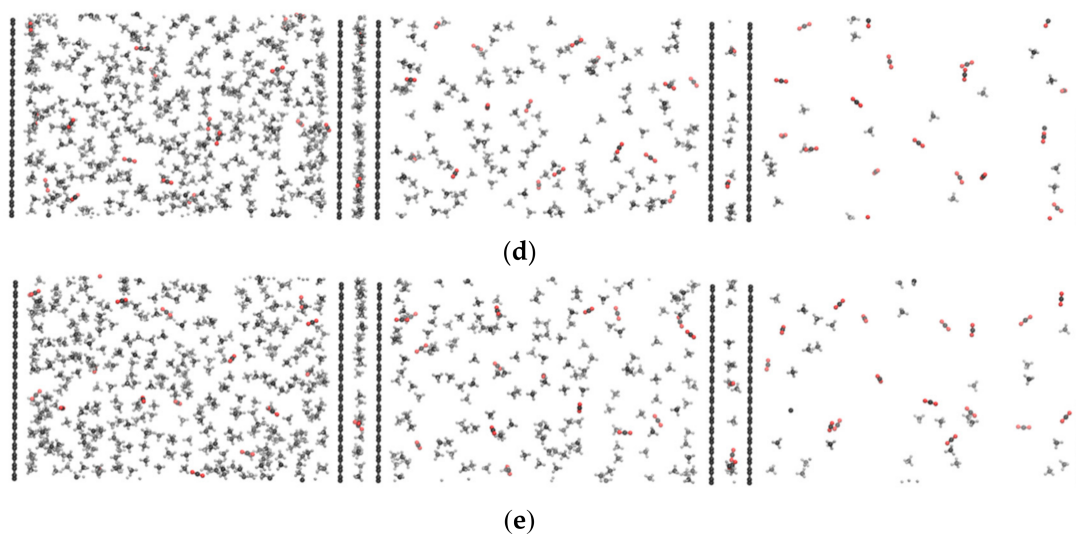
Figure 2. Snapshots from the time evolution of the inline configuration (W = 0) with the interlayer spacing of 8 Å within 4ns; from top to bottom: (**a**) 0 ns, (**b**) 1 ns, (**c**) 2 ns, (**d**) 3 ns, and (**e**) 4 ns.

The CO_2 molecules initially adsorb on the first membrane surface at the feed gas stream, as shown in Figure 2, and then cross the first membrane to the permeate side after saturating the surface and building up the adsorption layers. The CO_2 layers are built due to the repeated adsorption and desorption of CO_2 molecules on the membrane surface. Only one layer of CO_2 is built at the CH_4 composition of 80 mol% since a lower proportion of CO_2 molecules are present for membrane surface adsorption. In comparison, the permeation of CH_4 molecules through the first stage of the bilayer NPG membrane appears to be completely unhindered without any obvious surface adsorption of the CH_4 molecules. For the optimum separation efficiency of a membrane, high permeance and high selectivity are both needed. However, there is a trade-off between these factors in practice. For a given pore size, gas flux through membranes depends on the gaseous species' kinetic diameter and molecular weight, as well as the strength of their interactions with the membrane surface [42].

We applied three separate pore offset distances: inline (W = 0 Å), W = 10 Å, and W = 20 Å. To further examine the parameters influencing the permeation and separation performance, we also tested three interlayer distances of H = 8 Å, H = 12 Å, and H = 16 Å.

In this study, the molecular flow is used to describe the membrane's permeability quantitatively and is calculated according to the equation below [43].

$$F = \frac{N}{A \times t} \tag{1}$$

where F is the molecular flow (mol m^{-2} s^{-1}), N is the moles of gases crossing the membrane, A refers to the total membrane area (m^2), and t is the simulation time (s). For different configurations, the CO_2 flow and CH_4 flow after 4 ns of the simulation are shown in Figure 3.
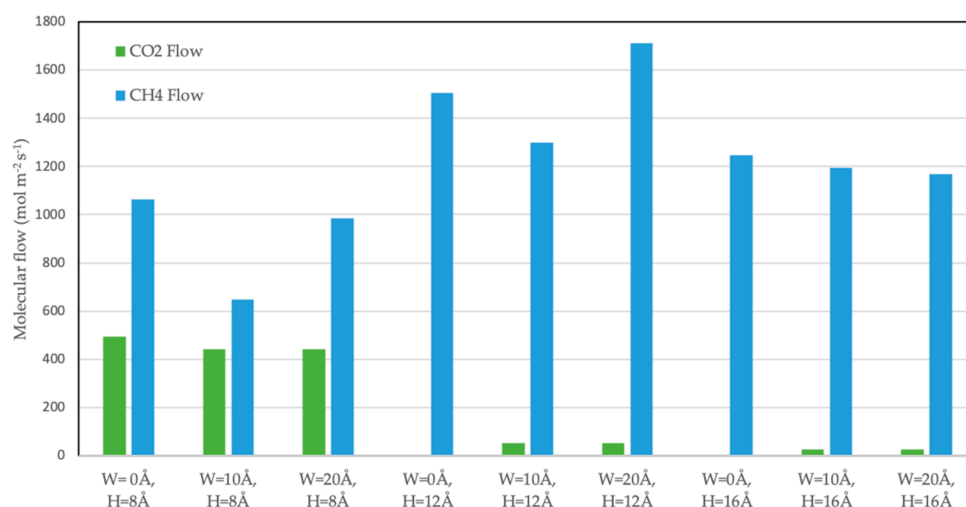
Figure 3. Molecular flow of CO_2 and CH_4 gases passing through two-stage bilayer NPG membranes for configurations with different pore offset distances (W), and interlayer spacings (H).

As shown in Figure 3, at a specified distance between layers, increasing the distance between the pores has little effect on carbon dioxide molecules' flow. In other words, under these conditions, the variation in the flow of carbon dioxide molecules is negligible. This trend is evident in all configurations with different interlayer distances. The flow of methane molecules is very much affected by the distance between the pores and the distance between the layers. At a certain distance between the pores, the methane flow in the configuration with H = 12 Å is more than that with H = 16 Å and H = 8 Å. Also, in a certain interlayer distance, the ratio of the flow of methane molecules to carbon dioxide molecules in linear configurations is more than other configurations with a distance between pores of 10 Å and 20 Å; as the distance between the pores increases, the length of the diffusion path of the molecules in the membranes increases. Also, by increasing the distance between the layers, these graphene layers' behavior changes from the membrane-like to bulk-like one.

In the configuration with an interlayer distance of 8 Å, the movement of molecules inside the membranes is somewhat limited, and as a result, the flow of molecules is reduced. By increasing this distance to 12 Å, molecules' freedom of movement within the membranes causes more molecules to pass through the membranes. However, by increasing the interlayer distance to 16 Å, these membranes' behavior is similar to that of a bulk region, causing molecules to move in these membranes in a larger environment. Also, in the 16Å interlayer distance, because the layers are farther apart and the system behavior is more similar to the bulk mode, the change in the distance between the pores loses its effect.
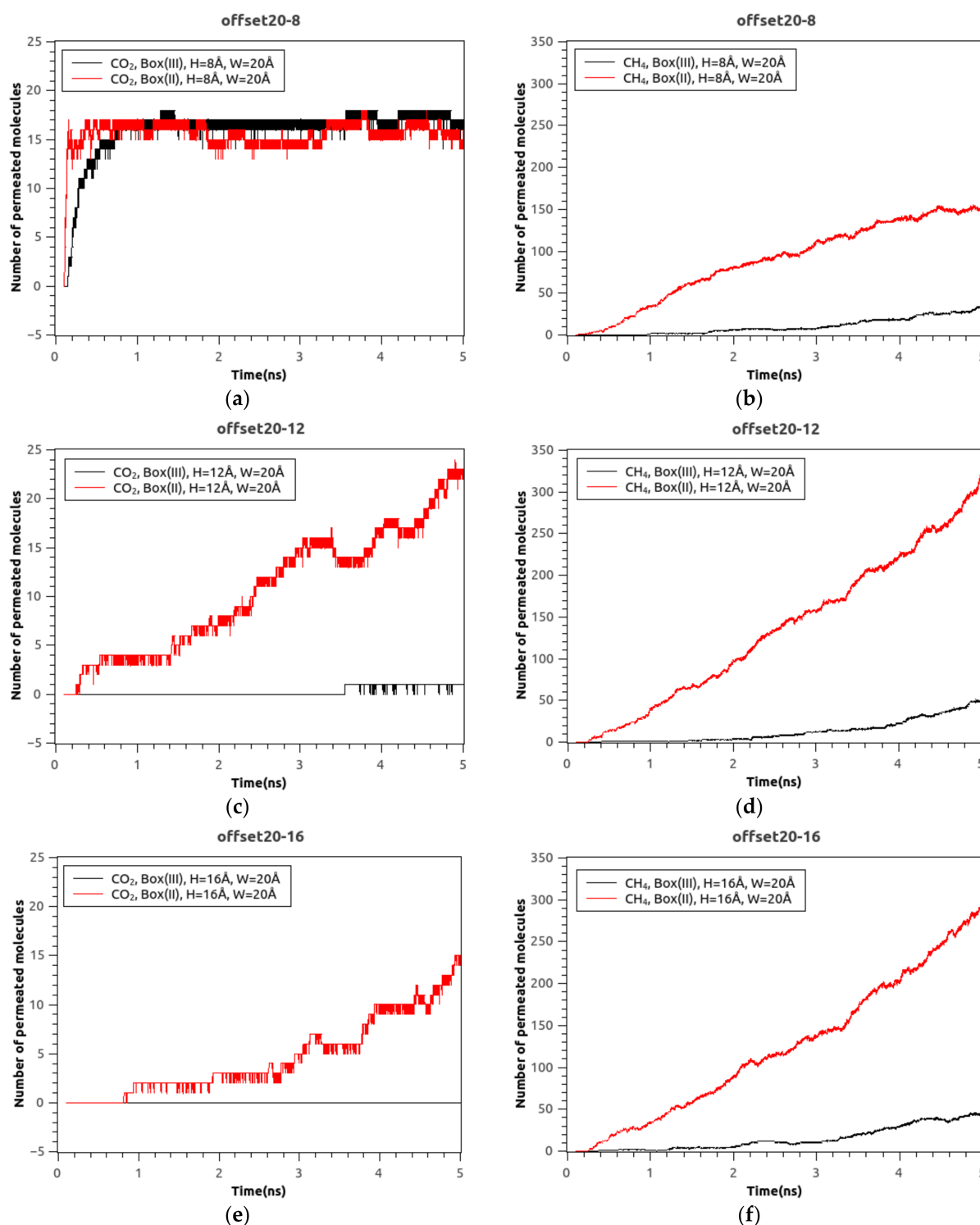
The number of permeated CO_2 and CH_4 molecules is monitored throughout the simulation. Figures 4–6 show the effect of the interlayer spacing (H = 8 Å, 12 Å, and 16 Å) on the number of CH_4 and CO_2 molecules passing through the first and second membranes (permeated to the chamber(II) and chamber (III), respectively), correspond to the configuration with pore offset distances of W = 0 Å, 10 Å, and 20 Å, respectively.
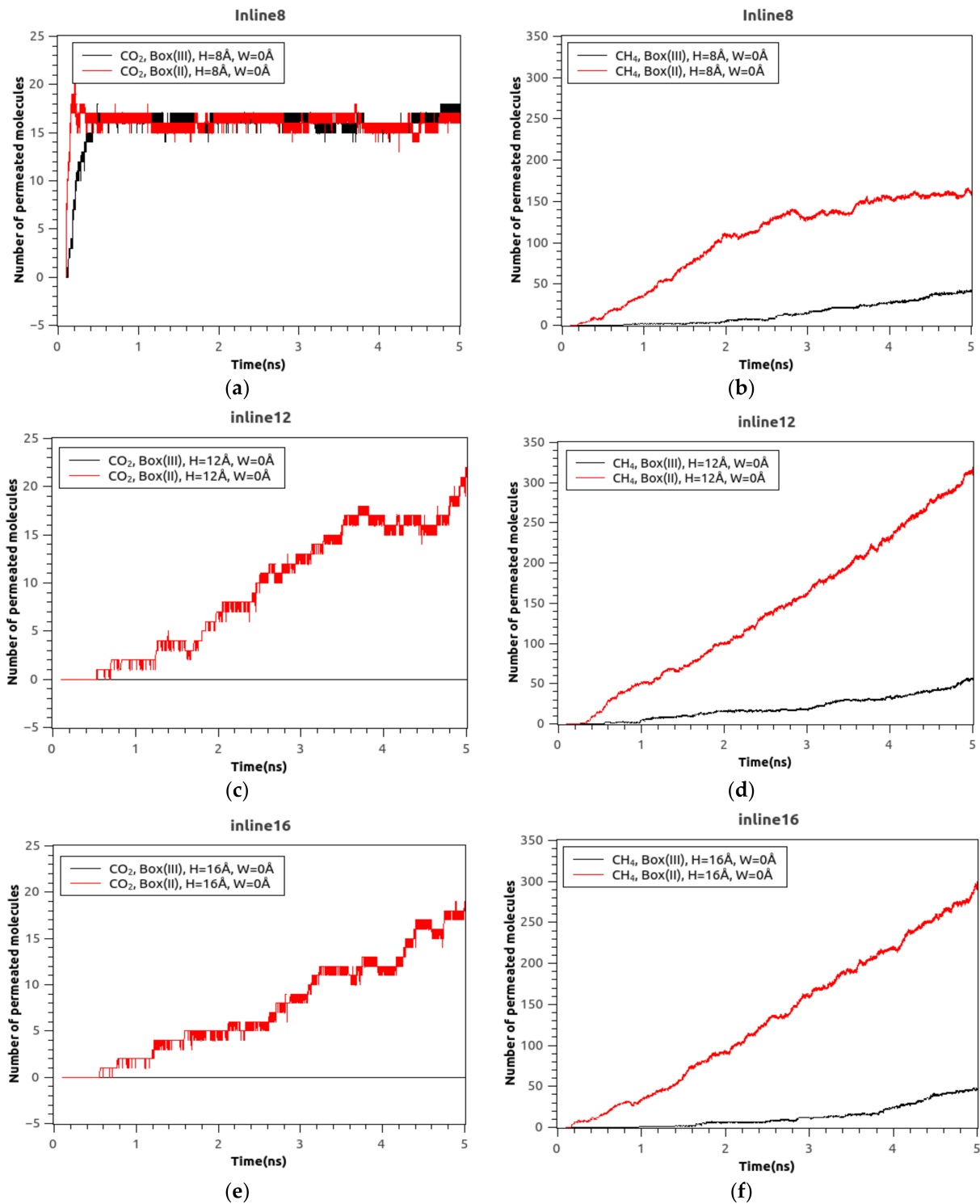
Figure 4. Time-varying number of molecules in the chamber(II) and chamber(III) permeated across the two-stage bilayer NPG for the inline configuration (W = 0 Å) of (**a**) CO_2, H = 8 Å (**b**) CH_4, H = 8 Å (**c**) CO_2, H = 12 Å (**d**) CH_4, H = 12 Å (**e**) CO_2, H = 16 Å (**f**) CH_4, H = 16 Å.
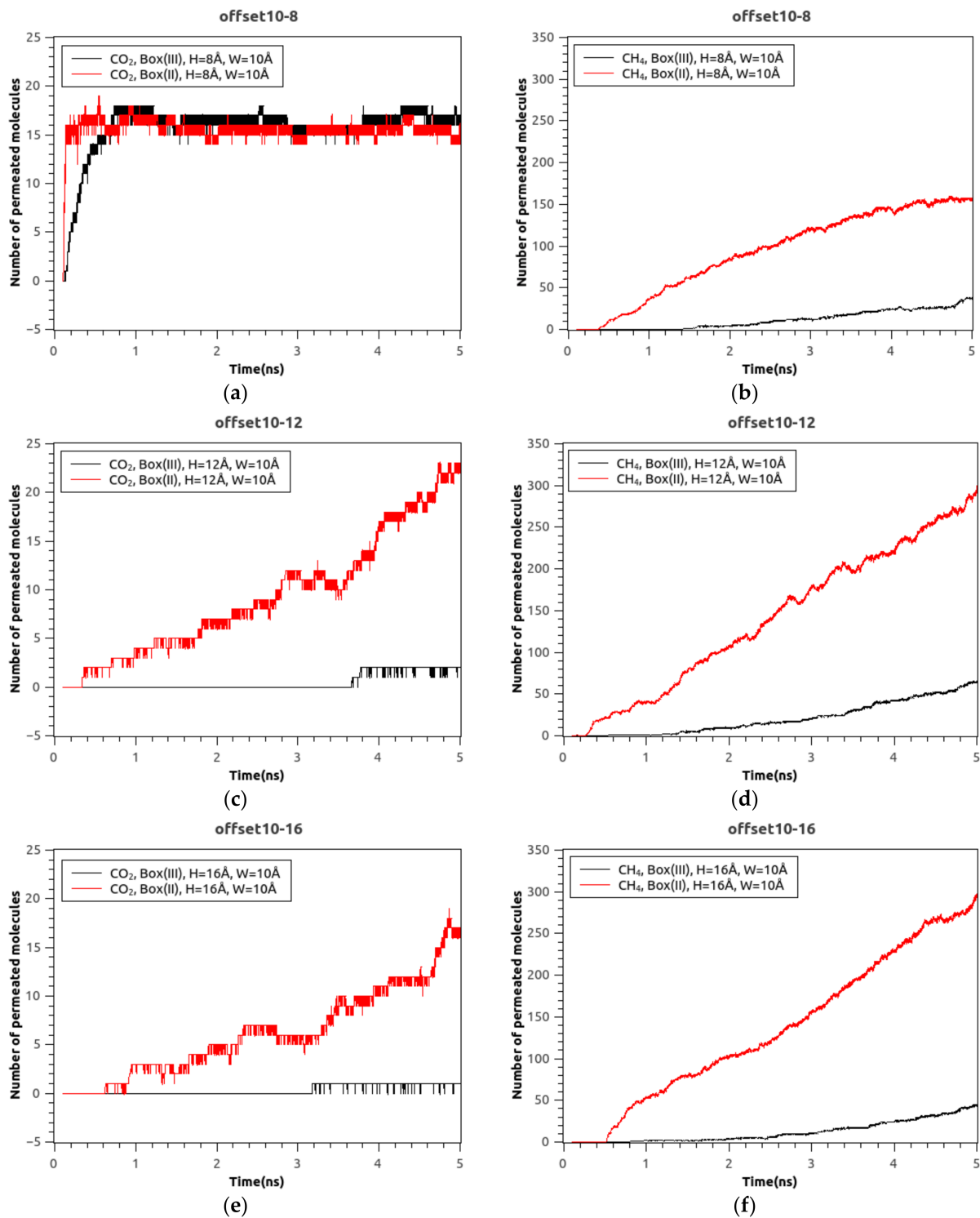
Figure 5. Time-varying number of molecules in the chamber(II) and chamber(III) permeated across the two-stage bilayer NPG for the configuration with W = 10 Å of (**a**) CO_2, H = 8 Å (**b**) CH_4, H = 8 Å (**c**) CO_2, H = 12 Å (**d**) CH_4, H = 12 Å (**e**) CO_2, H = 16 Å (**f**) CH_4, H = 16 Å.

Figure 6. Time-varying number of molecules in the chamber(II) and chamber(III) permeated across the two-stage bilayer NPG for the configuration with W = 20 Å of (**a**) CO_2, H = 8 Å (**b**) CH_4, H = 8 Å (**c**) CO_2, H = 12 Å (**d**) CH_4, H = 12 Å (**e**) CO_2, H = 16 Å (**f**) CH_4, H = 16 Å.

In all three figures, the number of CH_4 molecules crossing through the first membrane is significantly higher than that of the second membrane. The involvement of a second stage of the bilayer NPG membrane results in a substantial decrease in the number of permeated CO_2 into the chamber (III). It is noteworthy that the number of CO_2 molecules permeated into the chamber (II) while the interlayer spacing is 8 Å is approximately equal to the

number of molecules permeated into the chamber (III). The interlayer spacing to 12 Å is an ideal state for separating CO_2 and CH_4 gas mixture. As can be seen, the number of CO_2 molecules entering the second chamber increases, and at the same time, the number of CO_2 molecules entering the third chamber is significantly reduced. This interesting result for the interlayer distance is consistent with the experimental data for hydrated graphene systems (~12 Å) [40]. This observation indicates that according to MD's results, the interlayer spacing of 12 Å is a better choice for porous graphene multilayer membranes for better separation performance of CH_4 and CO_2 mixtures. For the interlayer distance of 16 Å, the system's behavior tends to be more like bulk than membrane behavior. As indicated in Figures 4–6, increasing the pore offset distance leads to a considerable decrease in the number of CO_2 molecules in the third chamber. In other words, the inline configuration is the most efficient one for CO_2 selectivity.

Moreover, configuration with zero pore offset distance (i.e., inline configuration) has the lowest permeance for CO_2 in the third chamber at the same interlayer distance. Since almost all CO_2 molecules are adsorbed on the feed and first permeate sides of the first bilayer NPG membrane (Figure 4b), there are not enough CO_2 molecules to cross the membrane.

We studied the CH_4/CO_2 mixture with 80 CH_4 mol%. Hence, all the above findings are because, at higher CH_4 concentrations, the likelihood of CO_2 molecules being carried through the membrane is higher. In other words, because the interactions of the CH_4-membrane are much weaker than those of the CO_2-membrane, the higher number of CH_4 molecules usually weakens the desirable interactions of the CO_2-membrane. Subsequently, the convective CO_2 mass transport dominates.

In this study, the CH_4/CO_2 separation selectivity is calculated instead of those of the CO_2/CH_4 separation because the permeation of CH_4 through the two-stage bilayer NPG membranes is higher than that of CO_2, as shown in Figures 4–6. The ratio of the individual permeances of the gases in the separation pair is historically known as membrane selectivity. The conventional definition can be simplified to the ratio of molecular content for systems in which both the feed gas and the permeate chambers are quite well combined (as indicated in Figure 2). The separation factor or selectivity of CH_4 over CO_2 for mixtures is defined as follows [44]:

$$S_{CH_4/CO_2} = \frac{\left(\frac{Y_{CH_4}}{Y_{CO_2}}\right)_{\text{Permeate stream}}}{\left(\frac{X_{CH_4}}{X_{CO_2}}\right)_{\text{Feed stream}}} \tag{2}$$

in which Y and X mean the molecules' mole fractions in the feed gas side and permeate side. In our investigation, the initial gas-phase CH_4/CO_2 ratio is 11. The effects of pore offset distance and interlayer spacing on the instantaneous membrane selectivity of the CH_4/CO_2 separation are given as a function of simulation time for the two-stage bilayer NPG membranes in Figures 7 and 8, respectively. As seen in these figures, the membrane selectivity increases with time for all configurations. However, the selectivity for the configurations with H = 12 Å is much larger than those with H = 8 Å and H = 16 Å.

Also, the selectivity of all membranes for the configurations with H = 12 Å and H = 16 Å is more than one, indicating that the separation efficiency of two-stage bilayer NPG membranes is satisfactory for the CH_4/CO_2 separation. However, the CH_4/CO_2 separation's selectivity is less than one for all their membrane configurations with H = 8 Å, suggesting that these NPG membranes are suitable for the CO_2/CH_4 rather than CH_4/CO_2 separation. As shown in Figure 7, the two-stage bilayer NPG membranes, in the configurations with H = 12 Å, exhibit a better separation efficiency for the CH_4/CO_2 mixture. The high affinity of the CO_2 molecules to the surface of the graphene membrane and pore rims may be the explanation for the improved performance with a larger interlayer spacing of the simulated NPG membrane.

All the abovementioned results demonstrate the selectivity of two-stage bilayer NPG membranes for CO_2 molecules. This study suggests one of the practical designs for the separation of CH_4 with the application in the CO_2 abatement industry.
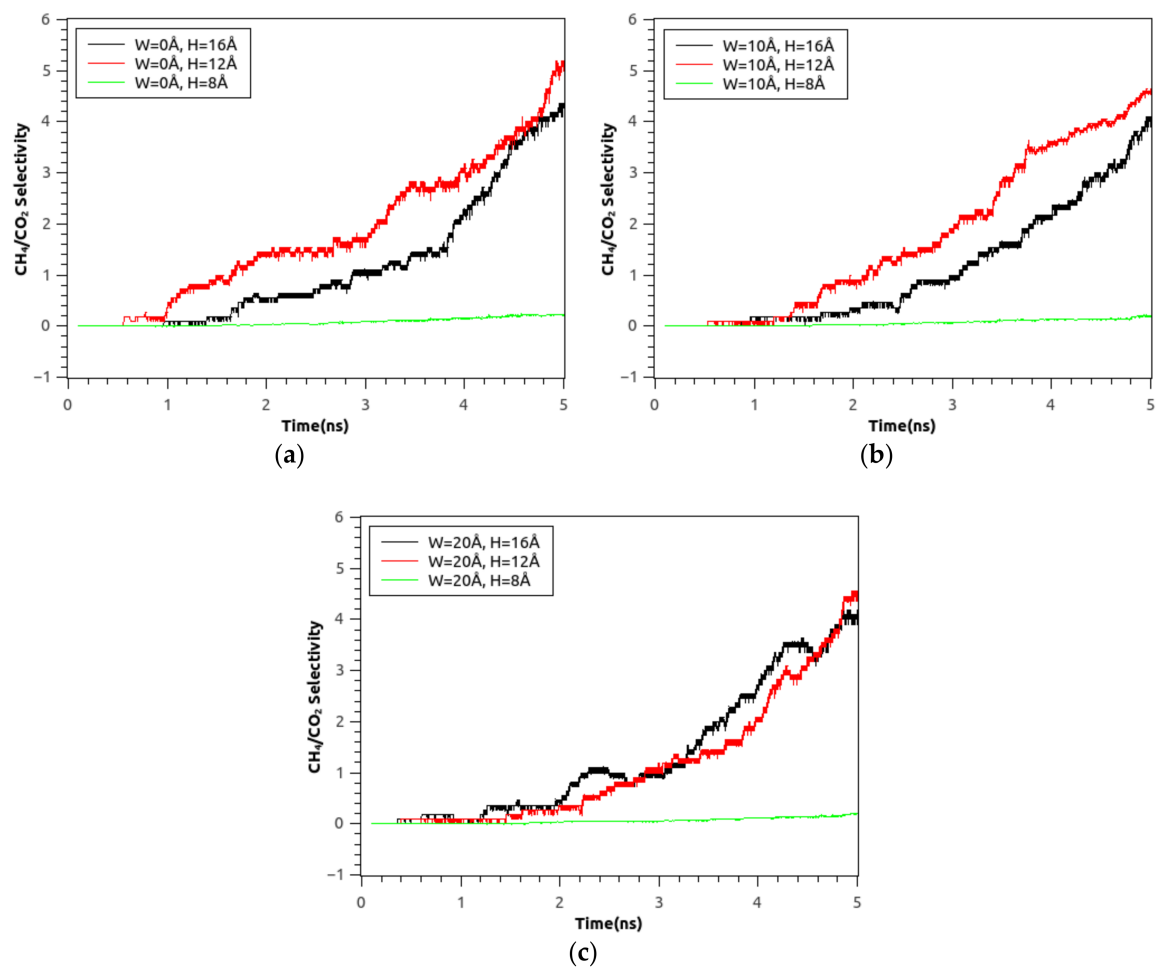
Figure 7. The effect of pore offset distance on the instantaneous CH_4/CO_2 selectivity as a function of simulation time (**a**) W = 0 Å (**b**) W = 10 Å (**c**) W = 20 Å.

Figure 8. *Cont.*

(**c**)
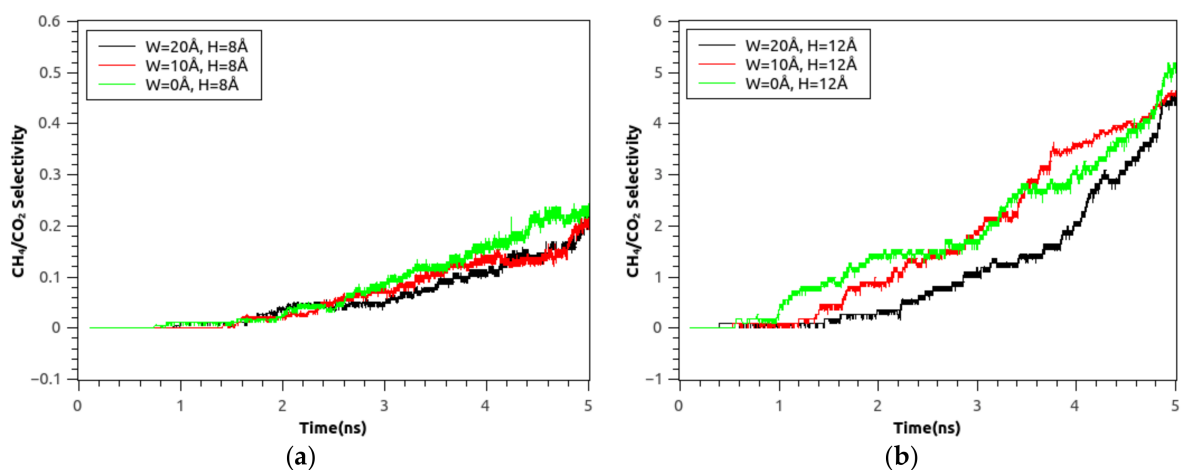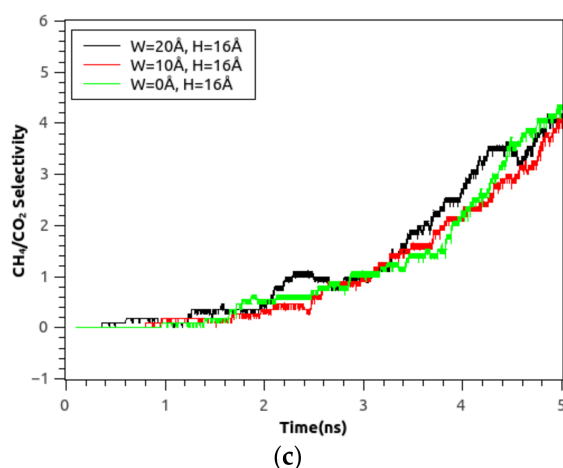
Figure 8. The effect of interlayer spacing on the instantaneous CH_4/CO_2 selectivity as a function of simulation time (**a**) H = 8 Å (**b**) H = 12 Å (**c**) H = 16 Å.

4. Conclusions

Graphene-based membranes are promising structures for the development of efficient gas separation. In this context, we investigated the permeation and separation performance of CH_4/CO_2 gas mixture crossing through a two-stage bilayer NPG membrane using molecular dynamics simulation. We examined the simultaneous effect of the offset distance and interlayer spacing on the performance of two-stage bilayer NPG membrane designs. The results show that configurations with an interlayer distance of 12 Å have the best performance in terms of separation and CH_4/CO_2 selectivity. This result is in good agreement with the experimental results for graphene membranes. Separation performance is also improved by applying the two-stage concept in bilayer membranes. We expect that by developing NPG membrane designs, it will be possible to provide a revolutionary and high-performance membrane separation technology for gas-separation processes.

Author Contributions: J.R.M. and C.R.M. conceived the project and were in charge of overall direction, funding, and planning. All authors contribute to design the molecular model and the computational framework and analyzed the data. N.R. carried out the molecular simulations, with help from A.K. N.R. wrote the manuscript with input from all authors. All authors have read and agreed to the published version of the manuscript.

Conflicts of Interest: The authors declare that there is no conflict of interest.

References

1. Li, Y.; Yi, H.; Tang, X.; Li, F.; Yuan, Q. Adsorption separation of CO_2/CH_4 gas mixture on the commercial zeolites at atmospheric pressure. *Chem. Eng. J.* **2013**, *229*, 50–56. [CrossRef]
2. Baker, R. Future directions of membrane gas-separation technology. *Membr. Technol.* **2001**, *2001*, 5–10. [CrossRef]

3. Gadipelli, S.; Guo, Z.X. Graphene-based materials: Synthesis and gas sorption, storage and separation. *Prog. Mater. Sci.* **2015**, *69*, 1–60. [CrossRef]

4. Alonso, A.; Moral-Vico, J.; Abo Markeb, A.; Busquets-Fité, M.; Komilis, D.; Puntes, V.; Sánchez, A.; Font, X. Critical review of existing nanomaterial adsorbents to capture carbon dioxide and methane. *Sci. Total Environ.* **2017**, *595*, 51–62. [CrossRef] [PubMed]

5. Suk, M.E.; Aluru, N.R. Molecular and continuum hydrodynamics in graphene nanopores. *RSC Adv.* **2013**, *3*, 9365–9372. [CrossRef]

6. Bunch, J.S.; Verbridge, S.S.; Alden, J.S.; Zande, A.M.; Parpia, J.M.; Craighead, H.G.; Mceuen, P.L. Impermeable Atomic Membranes from Graphene Sheets. *Nano Lett.* **2008**, *8*, 2458–2462. [CrossRef] [PubMed]

7. Humplik, T.; Lee, J.; O'Hern, S.C.; Fellman, B.A.; Baig, M.A.; Hassan, S.F.; Atieh, M.A.; Rahman, F.; Laoui, T.; Karnik, R.; et al. Nanostructured materials for water desalination. *Nanotechnology* **2011**, *22*, 292001. [CrossRef]

8. Xu, G.R.; Xu, J.M.; Su, H.C.; Liu, X.Y.; Lu-Li, X.; Zhao, H.L.; Feng, H.J.; Das, R. Two-dimensional (2D) nanoporous membranes with sub-nanopores in reverse osmosis desalination: Latest developments and future directions. *Desalination* **2019**, *451*, 18–34. [CrossRef]

9. Gharibzahedi, S.M.R.; Karimi-Sabet, J. Gas Separation in Nanoporous Graphene from Molecular Dynamics Simulation. *Chem. Prod. Process. Model.* **2016**, *11*, 29–33. [CrossRef]

10. Sint, K.; Wang, B.; Král, P. Selective ion passage through functionalized graphene nanopores. *J. Am. Chem. Soc.* **2008**, *130*, 16448–16449. [CrossRef]

11. Jiang, D.E.; Cooper, V.R.; Dai, S. Porous graphene as the ultimate membrane for gas separation. *Nano Lett.* **2009**, *9*, 4019–4024. [CrossRef]

12. Liu, H.; Chen, Z.; Dai, S.; Jiang, D.E. Selectivity trend of gas separation through nanoporous graphene. *J. Solid State Chem.* **2015**, *224*, 2–6. [CrossRef]

13. Tronci, G.; Raffone, F.; Cicero, G. Theoretical Study of Nanoporous Graphene Membranes for Natural Gas Purification. *Appl. Sci.* **2018**, *8*, 1547. [CrossRef]

14. Raghavan, B.; Gupta, T. H_2/CH_4 gas separation by variation in pore geometry of nanoporous graphene. *J. Phys. Chem. C* **2017**, *121*, 1904–1909. [CrossRef]

15. Yuan, Z.; Govind Rajan, A.; Misra, R.P.; Drahushuk, L.W.; Agrawal, K.V.; Strano, M.S.; Blankschtein, D. Mechanism and Prediction of Gas Permeation through Sub-Nanometer Graphene Pores: Comparison of Theory and Simulation. *ACS Nano* **2017**, *11*, 7974–7987. [CrossRef]

16. Wang, Y.; Yang, Q.; Li, J.; Yang, J.; Zhong, C. Exploration of nanoporous graphene membranes for the separation of N_2 from CO_2: A multi-scale computational study. *Phys. Chem. Chem. Phys.* **2016**, *18*, 8352–8358. [CrossRef]

17. Wu, T.; Xue, Q.; Ling, C.; Shan, M.; Liu, Z.; Tao, Y.; Li, X. Fluorine-modified porous graphene as membrane for CO_2/N_2 separation: Molecular dynamic and first-principles simulations. *J. Phys. Chem. C* **2014**, *118*, 7369–7376. [CrossRef]

18. Span, R.; Wagner, W. A new equation of state for carbon dioxide covering the fluid region from the triple-point temperature to 1100 K at pressures up to 800 MPa. *J. Phys. Chem. Ref. Data* **1996**, *25*, 1509–1596. [CrossRef]

19. Sun, C.; Wen, B.; Bai, B. Application of nanoporous graphene membranes in natural gas processing: Molecular simulations of CH_4/CO_2, CH_4/H_2S and CH_4/N_2 separation. *Chem. Eng. Sci.* **2015**, *138*, 616–621. [CrossRef]

20. Sun, C.; Bai, B. Improved CO_2/CH_4 Separation Performance in Negatively Charged Nanoporous Graphene Membranes. *J. Phys. Chem. C* **2018**, *122*, 6178–6185. [CrossRef]

21. Khakpay, A.; Rahmani, F.; Nouranian, S.; Scovazzo, P. Molecular Insights on the CH_4/CO_2 Separation in Nanoporous Graphene and Graphene Oxide Separation Platforms: Adsorbents versus Membranes. *J. Phys. Chem. C* **2017**, *121*, 12308–12320. [CrossRef]

22. Heidaryan, E. A note on model selection based on the percentage of accuracy-precision. *J. Energy Resour. Technol.* **2019**, *141*. [CrossRef]

23. Ang, E.Y.M.; Toh, W.; Yeo, J.; Lin, R.; Liu, Z.; Geethalakshmi, K.R.; Ng, T.Y. A review on low dimensional carbon desalination and gas separation membrane designs. *J. Membr. Sci.* **2020**, *598*, 117785. [CrossRef]

24. Fatemi, S.M.; Fatemi, S.J.; Abbasi, Z. Gas separation using graphene nanosheet: Insights from theory and simulation. *J. Mol. Model.* **2020**, *26*, 1–15. [CrossRef] [PubMed]

25. Yang, T.; Lin, H.; Zheng, X.; Loh, K.P.; Jia, B. Tailoring pores in graphene-based materials: From generation to applications. *J. Mater. Chem. A* **2017**, *5*, 16537–16558. [CrossRef]

26. Lee, X.J.; Hiew, B.Y.Z.; Lai, K.C.; Lee, L.Y.; Gan, S.; Thangalazhy-Gopakumar, S.; Rigby, S. Review on graphene and its derivatives: Synthesis methods and potential industrial implementation. *J. Taiwan Inst. Chem. Eng.* **2019**, *98*, 163–180. [CrossRef]

27. Malekian, F.; Ghafourian, H.; Zare, K.; Sharif, A.A.; Zamani, Y. Recent progress in gas separation using functionalized graphene nanopores and nanoporous graphene oxide membranes. *Eur. Phys. J. Plus* **2019**, *134*, 1–12. [CrossRef]

28. Hauser, A.W.; Schwerdtfeger, P. Methane-selective nanoporous graphene membranes for gas purification. *Phys. Chem. Chem. Phys.* **2012**, *14*, 13292–13298. [CrossRef]

29. Koenig, S.P.; Wang, L.; Pellegrino, J.; Bunch, J.S. Selective molecular sieving through porous graphene. *Nat. Nanotechnol.* **2012**, *7*, 728–732. [CrossRef]

30. Jorgensen, W.L.; Maxwell, D.S.; Tirado-Rives, J. Development and testing of the OPLS all-atom force field on conformational energetics and properties of organic liquids. *J. Am. Chem. Soc.* **1996**, *118*, 11225–11236. [CrossRef]

31. Potoff, J.J.; Siepmann, J.I. Vapor-liquid equilibria of mixtures containing alkanes, carbon dioxide, and nitrogen. *AIChE J.* **2001**, *47*, 1676–1682. [CrossRef]

32. Plimpton, S. Fast parallel algorithms for short-range molecular dynamics. *J. Comput. Phys.* **1995**, *117*, 1–19. [CrossRef]

33. Surwade, S.P.; Smirnov, S.N.; Vlassiouk, I.V.; Unocic, R.R.; Veith, G.M.; Dai, S.; Mahurin, S.M. Water desalination using nanoporous single-layer graphene. *Nat. Nanotechnol.* **2015**, *10*, 459–464. [CrossRef] [PubMed]

34. Celebi, K.; Buchheim, J.; Wyss, R.M.; Droudian, A.; Gasser, P.; Shorubalko, I.; Kye, J.-I.; Lee, C.; Park, H.G. Ultimate permeation across atomically thin porous graphene. *Science* **2014**, *344*, 289–292. [CrossRef] [PubMed]

35. O'Hern, S.C.; Boutilier, M.S.H.; Idrobo, J.C.; Song, Y.; Kong, J.; Laoui, T.; Atieh, M.; Karnik, R. Selective ionic transport through tunable subnanometer pores in single-layer graphene membranes. *Nano Lett.* **2014**, *14*, 1234–1241. [CrossRef]

36. Fan, Z.; Zhao, Q.; Li, T.; Yan, J.; Ren, Y.; Feng, J.; Wei, T. Easy synthesis of porous graphene nanosheets and their use in supercapacitors. *Carbon* **2012**, *50*, 1699–1703. [CrossRef]

37. Fox, D.; O'Neill, A.; Zhou, D.; Boese, M.; Coleman, J.N.; Zhang, H.Z. Nitrogen assisted etching of graphene layers in a scanning electron microscope. *Appl. Phys. Lett.* **2011**, *98*, 243117. [CrossRef]

38. Bieri, M.; Treier, M.; Cai, J.; Aït-Mansour, K.; Ruffieux, P.; Gröning, O.; Gröning, P.; Kastler, M.; Rieger, R.; Feng, X.; et al. Porous graphenes: Two-dimensional polymer synthesis with atomic precision. *Chem. Commun.* **2009**, 6919–6921. [CrossRef]

39. Fischbein, M.D.; Drndić, M. Electron beam nanosculpting of suspended graphene sheets. *Appl. Phys. Lett.* **2008**, *93*, 2006–2009. [CrossRef]

40. Stankovich, S.; Dikin, D.A.; Piner, R.D.; Kohlhaas, K.A.; Kleinhammes, A.; Jia, Y.; Wu, Y.; Nguyen, S.T.; Ruoff, R.S. Synthesis of graphene-based nanosheets via chemical reduction of exfoliated graphite oxide. *Carbon* **2007**, *45*, 1558–1565. [CrossRef]

41. Gogoi, A.; Konch, T.J.; Raidongia, K.; Anki Reddy, K. Water and salt dynamics in multilayer graphene oxide (GO) membrane: Role of lateral sheet dimensions. *J. Membr. Sci.* **2018**, *563*, 785–793. [CrossRef]

42. Sun, C.; Boutilier, M.S.H.; Au, H.; Poesio, P.; Bai, B.; Karnik, R.; Hadjiconstantinou, N.G. Mechanisms of molecular permeation through nanoporous graphene membranes. *Langmuir* **2014**, *30*, 675–682. [CrossRef] [PubMed]

43. Tao, Y.; Xue, Q.; Liu, Z.; Shan, M.; Ling, C.; Wu, T.; Li, X. Tunable hydrogen separation in porous graphene membrane: First-principle and molecular dynamic simulation. *ACS Appl. Mater. Interfaces* **2014**, *6*, 8048–8058. [CrossRef] [PubMed]

44. Wall, Y.; Braun, G.; Kaltenborn, N.; Voigt, I.; Brunner, G. Separation of CO_2/N_2 by Means of a Carbon Membrane. *Chem. Eng. Technol.* **2012**, *35*, 508–512. [CrossRef]